Northern East Asian Monsoon Precipitation Revealed by Airmass Variability and Its Prediction

KYONG-HWAM SEO AND JUN-HYEOK SON

Department of Atmospheric Sciences, Division of Earth Environmental Systems, Pusan National University, Busan, South Korea

JUNE-YI LEE

Research Center for Climate Sciences, Pusan National University, Busan, South Korea

HYO-SEOK PARK

Korea Institute of Geoscience and Mineral Resources, Daejeon, South Korea

(Manuscript received 22 July 2014, in final form 9 February 2015)

ABSTRACT

This work provides a new perspective on the major factors controlling the East Asian summer monsoon (EASM) in July and a promising physical–statistical forecasting of the EASM ahead of summer. Dominant modes of the EASM are revealed from the variability of large-scale air masses discerned by equivalent potential temperature, and they are found to be dynamically connected with the anomalous sea surface temperatures (SSTs) over the three major oceans of the world and their counterparts of prevailing atmospheric oscillation or teleconnection patterns. Precipitation over northern East Asia (NEA) during July is enhanced by the tropical central Indian Ocean warming and central Pacific El Niño–related SST warming, the northwestern Pacific cooling off the coast of NEA, and the North Atlantic Ocean warming. Using these factors and data from the preceding spring seasons, the authors build a multiple linear regression model for seasonal forecasting. The cross-validated correlation skill predicted for the period 1994 to 2012 is up to 0.84, which far exceeds the skill level of contemporary climate models.

1. Introduction

The East Asian summer monsoon (EASM) is one of the most important large-scale circulation systems, significantly influencing weather and climate over the whole globe. In particular, understanding of the EASM is crucial for agricultural, industrial, environmental, and recreational activities, as well as for the prevention of natural disasters. The EASM exhibits significant interannual variation, of which the dominant factors are not fully understood (Lau et al. 2000; Wu et al. 2009). In addition, prediction of EASM precipitation based on contemporary numerical global models remains unreliable (Chen et al. 2013; Yang et al. 2008; Wang et al. 2005; Webster et al. 1998). For example, our calculations demonstrate that the state-of-the-art global atmosphere–ocean coupled forecast models, such as the Australian Bureau of Meteorology model (ABOM) system, the GFDL, and the NCEP CFSv2, have a correlation skill of only 0.04–0.28 over the EASM rainfall region (averaged over 31.25°–41.25°N, 116.25°–141.25°E) for 1- or 2-month lead forecasts for July precipitation (Fig. 1). In contrast, the forecast skill for the Indian and western North Pacific summer monsoon is much greater, because of the understanding of the related physical processes (air–sea interaction and equatorial wave dynamics; Xie et al. 2009; Wang et al. 2000) and improvement of global climate models in representing the tropical atmospheric and oceanic variability.

The EASM rainband migrates from about 20° to 40°N during the boreal summer season according to the slow (sometimes abrupt) latitudinal movement of the mei-yu–changma–baiu front (Wang and LinHo 2002). The

Corresponding author address: Dr. Kyong-Hwan Seo, Department of Atmospheric Sciences, Pusan National University, Busan 609735, South Korea.
E-mail: khseo@pusan.ac.kr

DOI: 10.1175/JCLI-D-14-00526.1

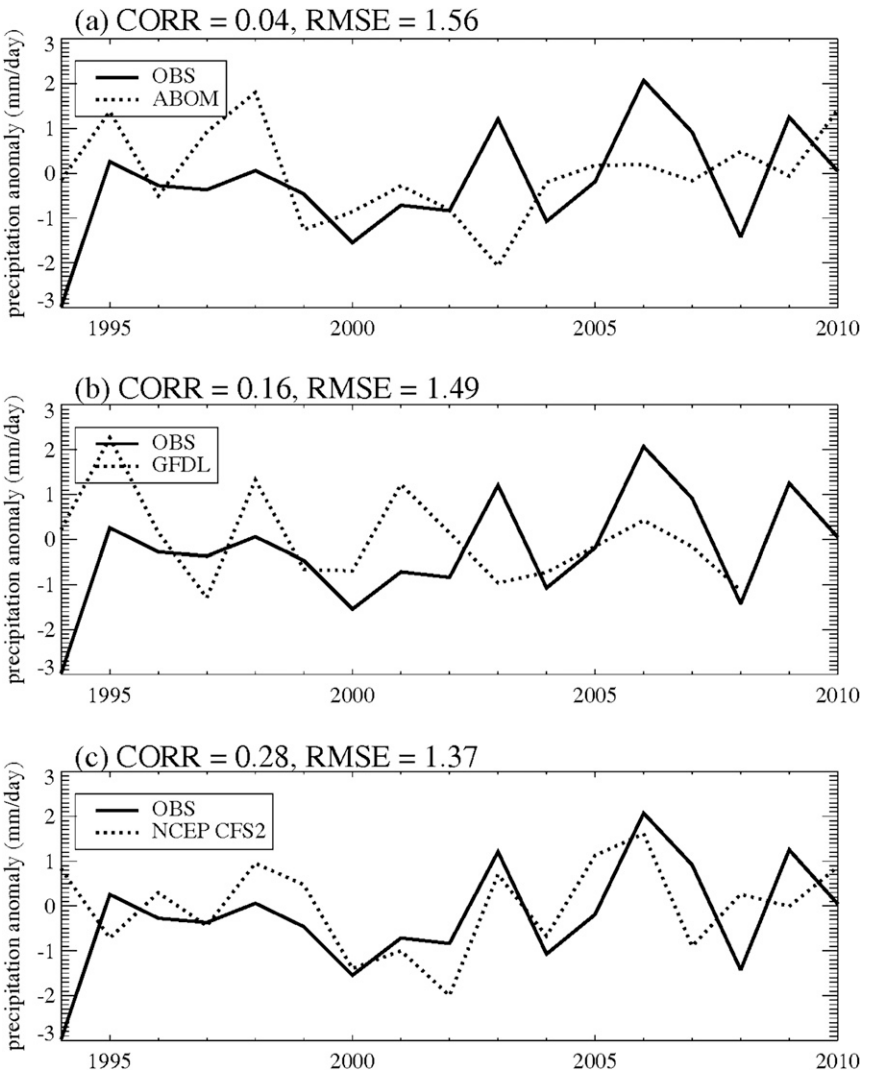

FIG. 1. Precipitation anomaly (mm day^{-1}) during July over northern East Asia (31.25°–41.25°N, 116.25°–141.25°E), forecasted from the following three atmosphere–ocean coupled models initialized in the month of May: (a) ABOM, (b) GFDL, and (c) NCEP CFSv2.

southern part (25°–31°N) of the East Asian region experiences a huge amount of rainfall from May to June (Zhao et al. 2007). The northern part (31.25°–41.25°N) of the EASM region exhibits a peak rainfall and its standard deviation maxima in July (Seo et al. 2012; Fig. 2). A considerable amount of rainfall also occurs in August, usually owing to typhoon and local convective activities. Consequently, the June–August (JJA) seasonal mean precipitation is determined by a mixed feature of each month. Furthermore, the interannual correlations among time series of EASM precipitation during June, July, and August are not very significant (not shown). Because of this, it is expected that a physical mechanism of the EASM is disparate for each month; therefore, for a detailed investigation of the EASM characteristics, June, July, and August should be considered separately.

In this study, we analyze mechanisms for the interannual variability of air mass and monsoonal front over northern East Asia (NEA) during July, when the monsoon front affects the highly populated East Asia region (including China, Korea, and Japan) and peak precipitation occurs over NEA. We perform an empirical orthogonal function (EOF) analysis on equivalent potential temperature (EPT), since EPT field represents large-scale airmass distribution. Using this variable is advantageous because it possesses much larger spatial and temporal scales than precipitation and considers temperature and humidity together. Essentially, the strong gradient of EPT implies different air masses.

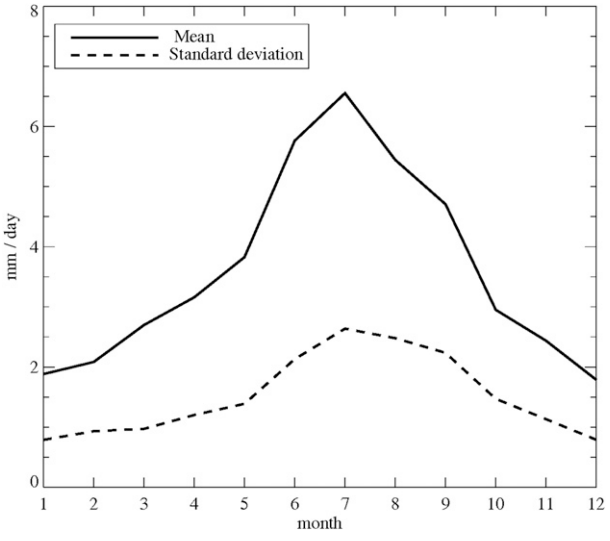

FIG. 2. Climatological monthly mean precipitation (thick line, mm day^{-1}) and its standard deviation (dashed line, mm day^{-1}) averaged in the northern East Asia domain (31.25°–41.25°N, 116.25°–141.25°E).

Therefore, the EASM front can be explicitly detected as the demarcation of two different air masses along which the strong meridional gradient of EPT appears (Tomita et al. 2011; Fig. 3).

The other advantage of this EPT, or airmass, approach is that EPT variation is closely related to precipitation variation since a large amount of precipitation occurs along the monsoonal front, which, as mentioned above, can be described by the strong EPT gradient. In fact, stronger EPT gradient appears to induce stronger mei-yu precipitation, as shown in Zhao et al. (2004, 2010). In this study, instead of directly performing an EOF analysis on NEA precipitation fields, the precipitation variation is estimated through airmass variation. In fact, it is extremely difficult to investigate precipitation variation using circulation-based EASM indices. For example, Wang and Fan's (1999) circulation index (U850 for 5°–15°N, 90°–130°E minus U850 for 22.5°–32.5°N, 110°–140°E), which is considered the most effective index for the estimation of EASM variation, correlates with precipitation over NEA (31.25°–41.25°N, 116.25°–141.25°E) only at ~0.25 because this index seems to be representative for a more subtropical monsoon system, or at least a more southern monsoonal region, than NEA. To overcome this difficulty, a unified East Asian monsoon index is devised, using precipitation and several atmospheric circulation variables (Wang et al. 2008). However, this index is also mainly determined by circulation variations; for example, the correlation coefficient with the Wang and Fan (1999) index amounts to −0.97. Consequently exact processes in the variations of the monsoonal precipitation are difficult to investigate from the dynamical variables. The EPT approach will provide new insight on this.

Based on the investigation of the most dominant physical mechanisms associated with the interannual variation of monsoonal front or precipitation, we developed a statistical model for the prediction of NEA precipitation. A multivariable linear regression model was developed by Wu et al. (2009) for the prediction of the EASM based on the above Wang and Fan (1999) index. This empirical model used predictors such as the North Atlantic Oscillation (NAO) and the decaying and developing phases of El Niño–Southern Oscillation (ENSO). We applied this model to the prediction of NEA rainfall, but it provided a very low correlation skill (~0.25). Therefore, previously developed statistical models are not very applicable to real prediction of precipitation over this area. Several recent studies have examined the statistical prediction of precipitation using SST anomalies. For example, Lee and Seo (2013) developed the empirical model for the prediction of the South Korea Changma precipitation using springtime SST anomalies over the Pacific and Atlantic Oceans. Gao and Xie (2014) used 8 different SST factors to forecast the extreme precipitation over the Yangtze River basin. Others also used the SST anomalies (sometimes with atmospheric variables) for the forecast of local precipitation such as monsoon rainfall in Nepal (Gillies et al. 2013) and seasonal rainfall over the African Sahel (Badr et al. 2014). However, the empirical forecast model based on the SST anomalies as predictors for NEA monsoon precipitation has not been developed.

In this study, the physical mechanisms for the interannual variation of EASM precipitation over NEA in July are investigated, and a physics-based seasonal statistical prediction model is developed using springtime predictors. Data and methods are described in section 2, and general circulation model and coupled model experiments are presented in section 3. Section 4 shows the physical mechanisms for the NEA monsoonal front and rainfall variability through airmass variability and the development of a statistical forecast model for the prediction of NEA precipitation. Section 5 summarizes the results.

2. Data and methods

The following monthly mean datasets (1979–2012) are used in this study: 1) NOAA Extended Reconstructed SST (ERSST, v3b; Smith et al. 2008), 2) Global Precipitation Climatology Project (GPCP) precipitation (Adler et al. 2003), and 3) NCEP–DOE Reanalysis 2 datasets in pressure levels (Kanamitsu et al. 2002).

An EOF analysis was performed on an 850-hPa EPT field over the East Asian domain (10~70°N, 80~180°E).

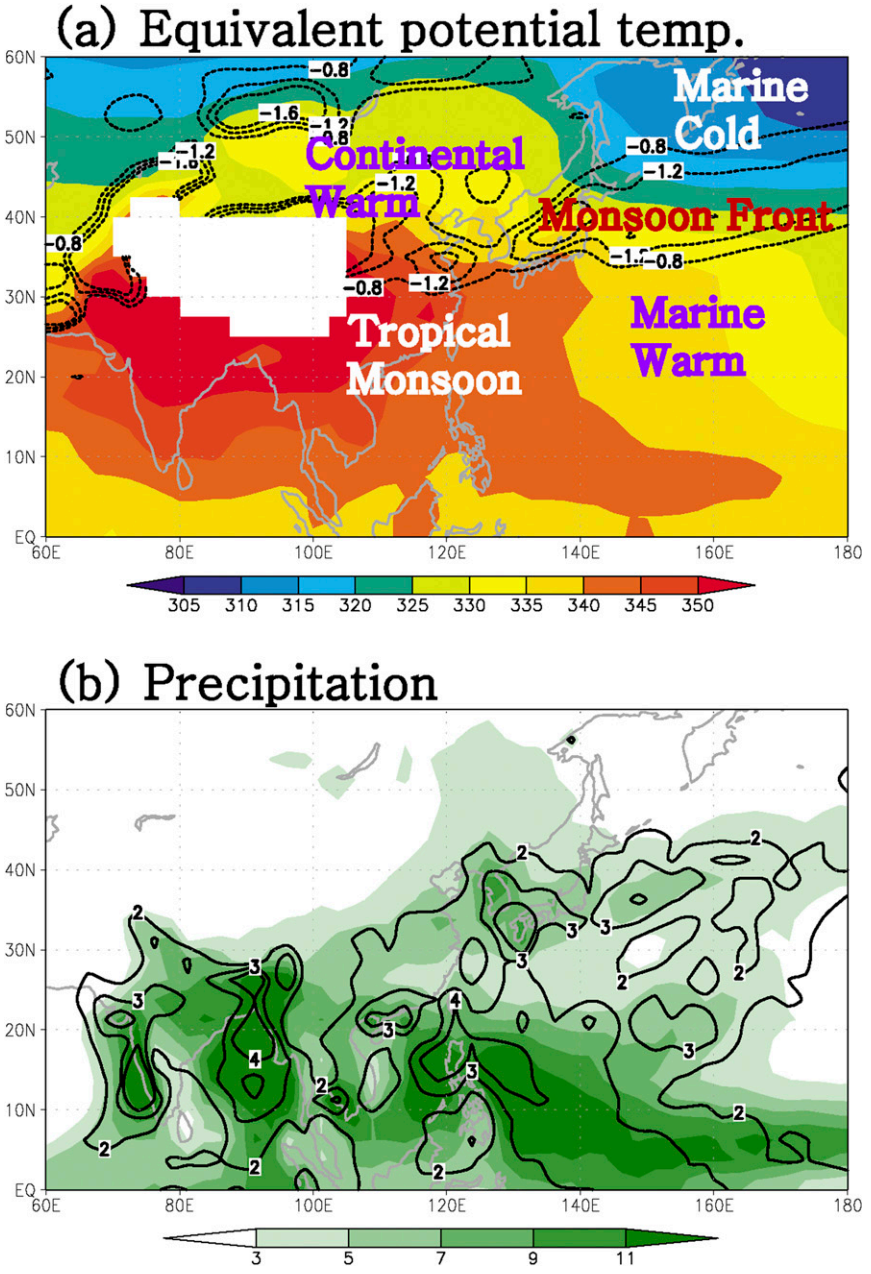

FIG. 3. Climatological mean (a) 850-hPa equivalent potential temperature (color, K) and its meridional gradient (dashed line, $\times 10^5$ K m^{-1}) and (b) precipitation (color, mm day^{-1}) and standard deviation (thick line, mm day^{-1}) during July.

To avoid the dominance of the tropical variance in the extraction of computational EOF modes, a correlation matrix was used by dividing covariance by standard deviations at each matrix element (instead of using a covariance matrix; Wang et al. 2008). An EOF analysis using a covariance matrix presents the regions with higher variance relative to the rest of the domain (Overland and Preisendorfer 1982). On the other hand, the EOF analysis using the correlation matrix can demonstrate the meridional confrontation of air masses along the midlatitudes. Therefore, North's rule of thumb (North et al. 1982) may not be an optimal estimation for the standard error in the correlation matrix. In this study, the Monte Carlo significance test was performed to evaluate the standard errors of eigenvalues. This was done by first prerandomizing the time sequence of each principal component (PC), next reconstructing the data, and finally reperforming the EOF analysis. The experiment was

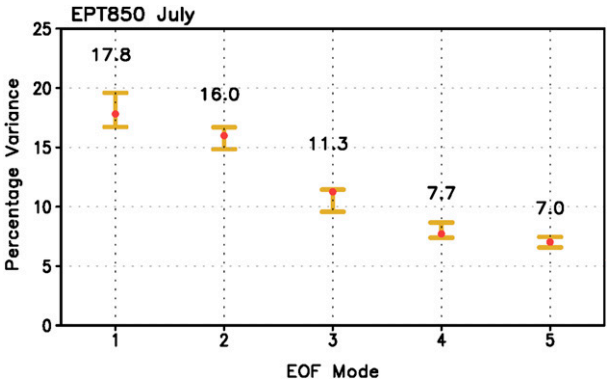

FIG. 4. Eigenvalues for the leading five modes and the related error bars at a 95% confidence level.

repeated 10 000 times (Fig. 4). The leading three EOFs are statistically independent of one another and are separated from the higher modes (4th and 5th).

An empirical model for the prediction of the precipitation over northern East Asia was developed for the period from 1994 to 2012. To prevent overfitting, Blockeel and Struyf (2002) suggested using 20%–30% of the data as test data and the remainder (70%–80%) as training data for performing regression and validation (Wu et al. 2009). Therefore, in this study, 4 years of data are ''successively'' left out as verification data.

3. Model experiments

Model experiments were designed to validate physical processes of each EOF mode.

A linear baroclinic model (LBM; Watanabe and Kimoto 2000) was used with a horizontal resolution of T42 and 20 vertical levels in sigma coordinates. Based on the linearized primitive equations, the LBM diagnoses steady-state atmospheric dynamical response to prescribed diabatic heating. Associated with the first two leading modes of the interannual variability in the NEA monsoon (which will be shown in the next section), atmospheric diabatic heating centered at 0°N, 160°E and 50°N, 135°E is forced to verify observed circulation patterns of the leading modes.

A coupled model is used when SST boundary forcing and air–sea interaction are important; for this study, we used the NCEP Climate Forecast System (CFS). As described in Seo and Wang (2010), the atmospheric component of the CFS model is the 2003 version of the Global Forecast System (GFS) model with a spectral truncation of T62 waves in the horizontal and a finite differencing in the vertical with 64 sigma layers. The oceanic component is the GFDL Modular Ocean Model version 3 (MOM3). For a more detailed description, please refer to Saha et al. (2006). In this study, the model integration started every January from 1984 to 1996 for the ensemble experiment. To verify the air–sea interaction process, which is important in maintaining the third mode in the EOF analysis (shown in the next section), SST fields with 2 K added to the climatological field are prescribed over the Indian Ocean (10°S~10°N, 50~100°E). A buffer zone is constructed for the horizontal boundaries. To show the anomaly fields, all quantities are subtracted from a control run forced by the climatological SST.

4. Results

a. *Physical mechanisms for NEA rainfall variability through air masses*

As mentioned in the introduction, the equivalent potential temperature represents large-scale air mass. The EASM quasi-stationary front is then characterized by the strong meridional gradient of EPT. Four different air masses are involved in the climatological EASM front (Fig. 3a): hot and humid tropical monsoonal air mass, marine warm air mass associated with the North Pacific subtropical high (NPSH), dry continental warm air mass over China, and marine cold air mass associated with the Okhotsk high. Climatological precipitation and its standard deviation maxima in the month of July appear over South Korea, Japan, and the far-western Pacific along 30°~35°N (Fig. 3b). The correlation coefficient between the precipitation and meridional gradient of EPT over the NEA frontal region (averaged over 31.25°–41.25°N, 116.25°–141.25°E) is as high as −0.72 in July during 1979–2012.

To understand the dominant modes related to the EASM, we conducted EOF analysis using 850-hPa EPT anomalies over the East Asian domain (10°–70°N, 80°–180°E) for the period 1979 to 2010. Prior to the analysis, a 9-point smoothing in space was applied to remove small-scale perturbations. Three leading modes, statistically independent of one another (Fig. 4), account for ~45% of the total variance (Fig. 5). The spatial pattern of the first mode shows confrontation between a cold air mass (negative EPT anomalies) from the Sea of Okhotsk and a warm, moist air mass (positive EPT anomalies) over the subtropical northwestern Pacific. The second mode features negative EPT anomalies over almost all East Asian regions (a negative trend in principal component 2 represents overall warming in the domain). The third mode displays a spatial pattern similar to the first mode over the northern latitudes (~40°–50°N), but the high-EPT air in south China intrudes into the low-EPT air mass along latitude 35°N to the east of Japan. The southeastern negative EPT anomaly forms as a western part of the NPSH, with considerably low specific humidity. It will be shown that the warm and humid air is transported to

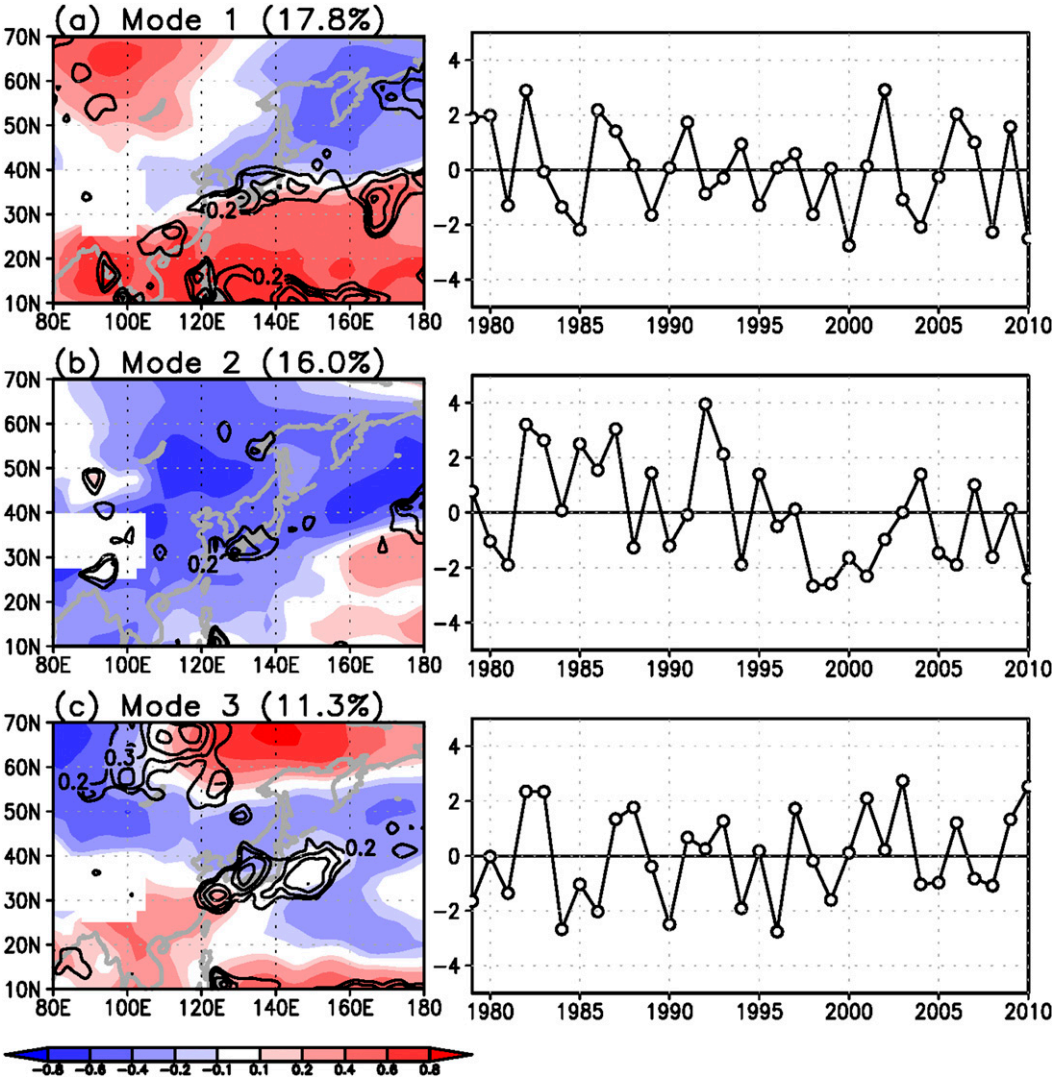

FIG. 5. (a) First, (b) second, and (c) third EOF spatial patterns of equivalent potential temperature (left panels; color) and corresponding PC time series (right panels). The correlation between the PC time series and precipitation is denoted by contours in the left panels. The first contour is 0.2 and the interval is 0.1. The fractional variance explained by each mode is shown in parentheses in the left panel.

the NEA area along the skirt of the NPSH to produce anomalous precipitation (Chang et al. 2000; Seo et al. 2013). Correlations with precipitation fields in the three modes (black contour) all illustrate a significant increase in precipitation over the NEA domain. Note that PC3 has the largest correlation value (0.54) compared to those of PC1 and PC2 (0.35 and 0.31, respectively). The time series of the principal components exhibit strong interannual variations with a prominent 2–4-yr fluctuation. PC2 also shows much slower trendlike variability.

Each of the EOF modes is dynamically linked to oceanic phenomena. Figure 6 shows the correlation fields of the sea surface temperature spanning the preceding winter and spring, the concurrent summer, and the following winter seasons for each EOF mode. Evidently, the first mode is related to the developing central Pacific (CP) El Niño (Yeh et al. 2009). The correlation coefficient between PC1 and the Niño-4 index is as high as 0.60 (Table 1). The related equatorial precipitation pattern (Fig. 7) demonstrates that the heating source over the central Pacific and cooling over the Maritime Continent induce Rossby and Kelvin waves, respectively, over the western equatorial Pacific. The Kelvin wave or heating over the CP tends to generate a meridionally propagating Rossby wave train over the western Pacific with a small cyclonic circulation anomaly at ~12°N, a larger anticyclonic circulation anomaly at ~25°N, and another cyclonic circulation anomaly at ~40°N. Therefore, this wave train

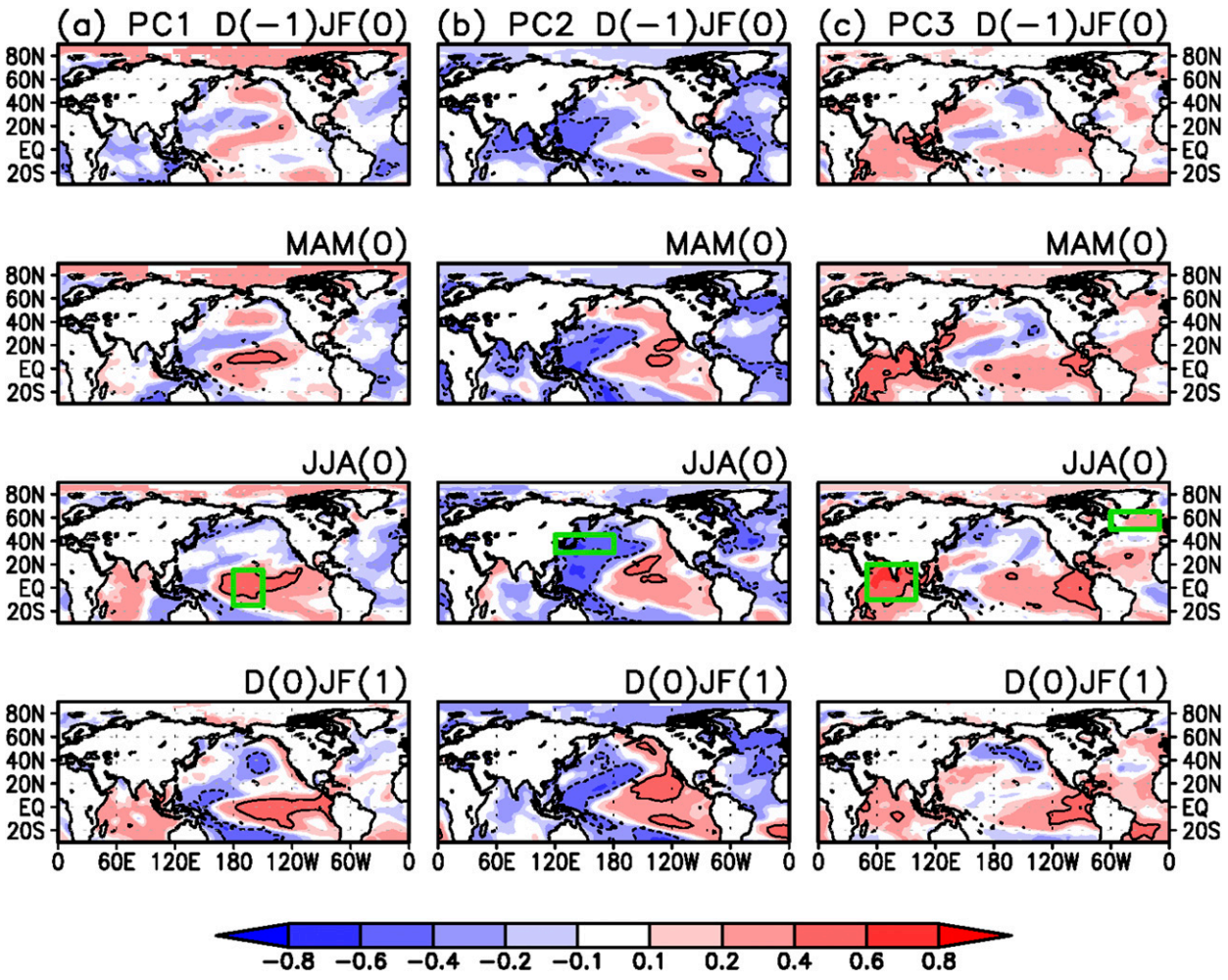

FIG. 6. Maps of correlation between SST anomalies and (a) PC1, (b) PC2, and (c) PC3, from the preceding winter to following winter (contour denotes the 90% confidence level; the Student's *t* test was used). The green boxes in the third row denote the areas of major SST anomalies used to construct the empirical model.

helps strengthen the NPSH and produces more intense southerlies or southwesterlies, generating precipitation along the east–west-directed monsoon front. A model simulation by LBM (Watanabe and Kimoto 2000), using the prescribed diabatic heating over the western tropical Pacific, reproduces this meridionally propagating Rossby wave train, including a prominent positive subtropical high anomaly (Fig. 10a).

The second mode has a strong relationship (correlation coefficient of 0.62, Table 1) with the positive phase of the Pacific decadal oscillation (PDO; Mantua et al. 1997). The PC including a linear trend gives a correlation of 0.73. Interannual variability is significant, as in Schneider and Cornuelle (2005), even if the primary PDO time scale is decadal to interdecadal. In the positive PDO phase, negative sensible heat flux from the colder sea surface leads to atmospheric cooling over NEA (Sun and Bryan 2010). The related lower and middle troposphere is characterized by a strong cyclonic cold anomaly centered at 40°N, 170°E and a relatively weaker anticyclonic warm anomaly to the south (Fig. 8), which is consistent with a previous study (Latif and Barnett 1996). The cold anomaly extends to the eastern Eurasian continent. This temperature configuration intensifies the meridional negative gradient in EPT over the NEA region, inducing a strengthening of instability

TABLE 1. Correlation coefficient between three PCs and the three oceanic indices (Niño-4, PDO, and IO SST anomalies) in July. Values exceeding the 99% confidence level are in bold. The Student's *t* test was used.

Indices	PC1	PC2	PC3
Niño-4 (5°S–5°N, 160°–210°E)	**0.60**	0.39	0.23
PDO	0.21	**0.62**	0.22
IO (15°S–15°N, 50°–100°E)	0.08	−0.19	**0.64**

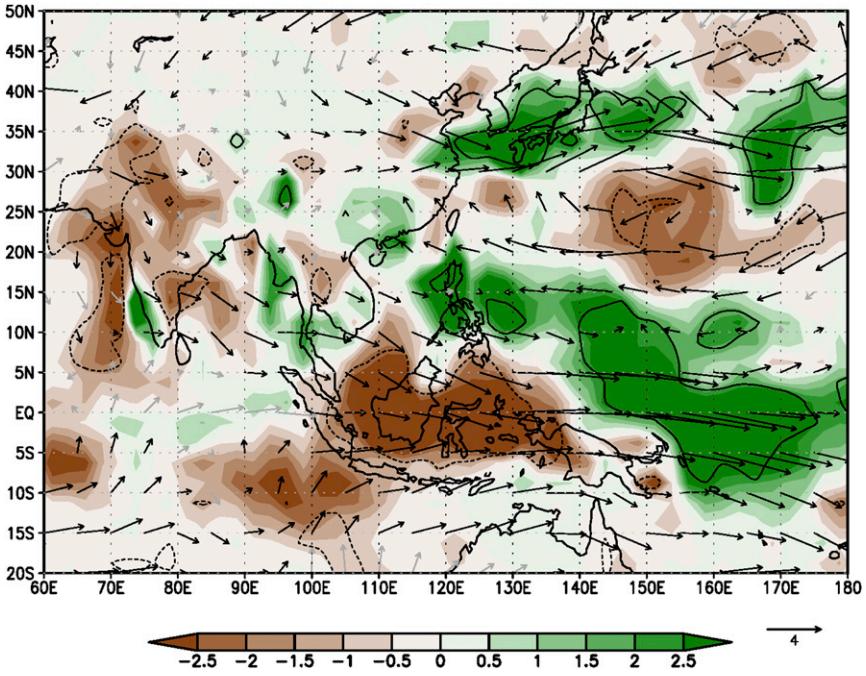

FIG. 7. Composite difference maps (strong-positive minus strong-negative cases) of precipitation (mm day^{-1}, color) and 850-hPa wind (m s^{-1}) associated with PC1. Strong-positive (-negative) cases are selected when the magnitude of PC1 is greater (less) than 1.0. Contours and black-vector winds denote significant anomalies at the 90% level.

and monsoon front that enhances precipitation. The northern cyclonic cold anomaly is likely the more important contributor. Enhanced baroclinicity induces the intensified upper-level jet stream by thermal wind balance, which in turn produces the stronger upper-level divergence. This is well known as a favorable condition for intense precipitation during the summer monsoon season. These anomalous circulation patterns are also retrieved by the LBM experiment where cold temperature forcing is prescribed over the NEA region (Fig. 10b).

The third mode correlates significantly ($r = 0.64$) with the Indian Ocean (IO) basinwide warming (Table 1). It is well known that this mode is associated with the decaying phase of the ENSO. More than 70% of El Niño events are followed by basinwide warming over the

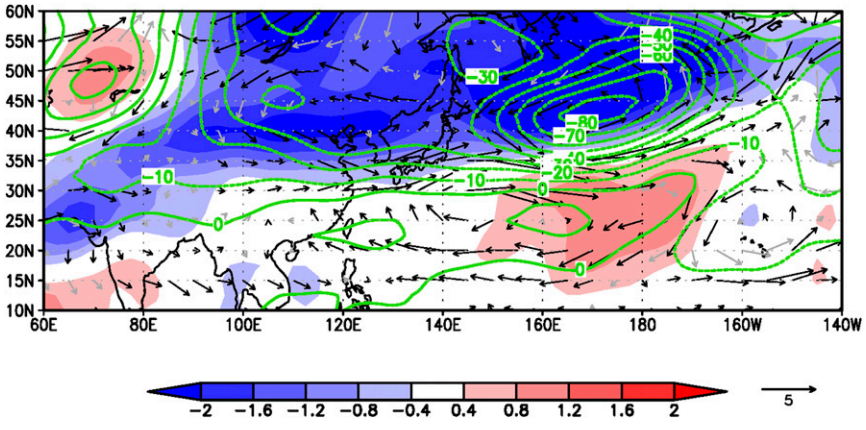

FIG. 8. Composite difference maps (strong-positive minus strong-negative cases) for 500-hPa geopotential height (gpm, green contour), 500-hPa air temperature (K, color), and 200-hPa wind (m s^{-1}, black vector at the 90% confidence level) associated with PC2. Contours and black-vector winds denote the significant anomalies at the 90% level.

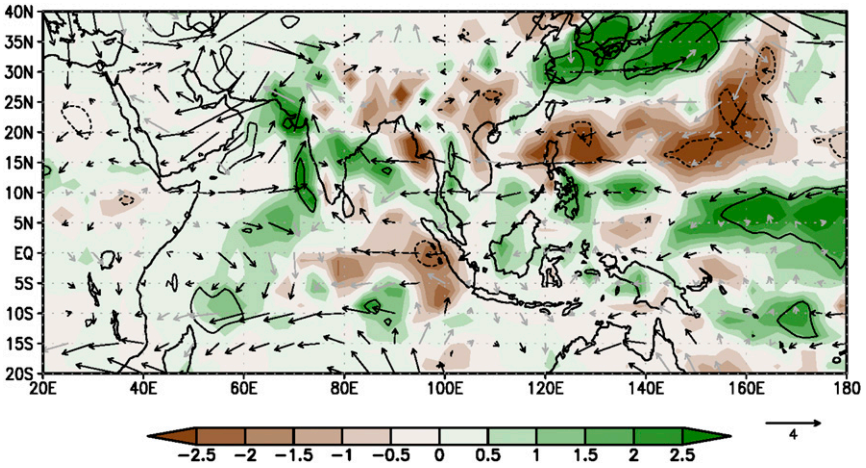

FIG. 9. Composite difference maps (strong-positive minus strong-negative cases) for precipitation (mm day^{-1}, color) and 500-hPa wind (m s^{-1}, vector) associated with PC3. Contours and black-vector winds denote significant anomalies at the 90% level.

tropical IO, peaking in spring (Yang et al. 2007). Close scrutiny of Fig. 9 reveals that precipitation and condensational heating occur mainly in the western equatorial and northern Indian Ocean. In particular, the strongest heating occurs over the Arabian Sea, similar to that reported by Yang et al. (2007). Accordingly, the zonal convergent flows take place along latitude 10°–15°N across the northern Indian Ocean and western Pacific, intensifying mean easterly trade winds over the western North Pacific (WNP; Wang et al. 2013; Jiang et al. 2013; Yang et al. 2007). The strengthening of the trade winds lowers the local SST over the WNP and reinforces the NPSH over this region (Fig. 9; Jiang et al. 2013; Wang et al. 2000; Wang et al. 2013), suggesting that the local air–sea interaction plays a role in the formation of this mode. Suppressed convection in the WNP in turn enhances EASM precipitation by a northward-propagating atmospheric Rossby wave train, producing the so-called Pacific–Japan teleconnection pattern (Nitta 1987). To verify this mechanism, an atmosphere–ocean coupled model (CFS; Saha et al. 2006) is used since, contrary to the first two modes, this mode occurs because of air–sea interaction (Fig. 10c). Warm SST forcing over the Indian Ocean evidently reproduces this strengthening of the NPSH (Fig. 10c) in the coupled model ensemble integration. [Note that an LBM experiment forced by diabatic heating over the Indian Ocean produces a much weaker NPSH signal, with the southern branch of the NPSH and the corresponding easterly winds along 15°–22.5°N not being simulated well (not shown). This is due to the absence of the air–sea interaction over the WNP region in the AGCM simulation.] This mode is also related to SST anomalies over the northern Atlantic Ocean via the NAO (Delworth 1996; Wu et al. 2009). Our calculation shows that precipitation correlates significantly (~0.4) with SST anomalies over the northern Atlantic Ocean. A previous study by Wu et al. (2009) demonstrated that the anomalous NAO in the preceding winter and spring can induce a tripolar SST pattern in the northern Atlantic Ocean (Czaja and Frankignoul 2002), which can persist through the following summer owing to the ocean memory effect. This excites downstream Rossby wave propagation across northern Eurasia, which modifies the pressure over NEA and to the southeast of NEA, thereby enhancing the EASM. The negative phase of the NAO is characterized by the positive SST anomalies over higher latitudes and the tropical Atlantic and by the negative SST anomalies in between; the related teleconnection by wave train is the development of the anticyclonic circulation anomalies centered to the southeast of Korea or south of Japan.

b. *Development of the statistical forecast model*

The above three modes are shown to be significantly related to slowly varying external forcing: SST anomalies over the central Pacific, the northwestern Pacific, the Indian Ocean, and the Atlantic. Use of these physical factors may facilitate improved empirical prediction for the NEA precipitation. We constructed a multivariable linear regression model to predict July precipitation using these four SST anomalies. All SST anomalies were domain averaged (Fig. 11) and normalized according to their respective standard deviations. In Fig. 11, labels A, B, and C indicate, respectively, the IO SST, NEA SST, and CP El Niño–related SST anomaly domains; D is the northernmost Atlantic SST anomaly of the three meridionally located SST cells because this northernmost

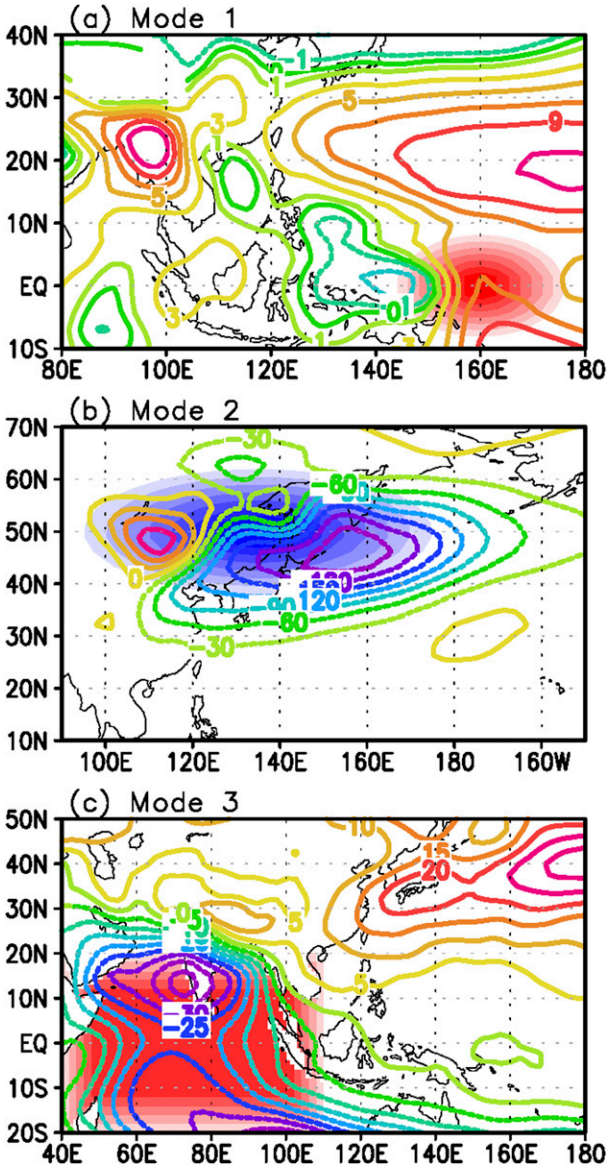

FIG. 10. Model experiments for the physical process of each mode. Contours show (a) 850-hPa, (b) 500-hPa, and (c) 850-hPa geopotential heights. The 3D diabatic heating in (a) and (b) (LBM) and the SST in (c) (CFS model) are used as the prescribed forcing (in shading). The CFS model is integrated from January to July and the average field for 12 ensemble members is plotted in (c).

cell plays the most crucial role in relation to the NAO (Watanabe and Kimoto 2000).

To avoid the possible complexity of an interdecadal variation of jet stream in western and northern China and Russia (Kwon et al. 2007) and to perform a prediction for future years with higher confidence, only the recent 19-yr data are used. Cross validation using a leave-4-years-out method (Blockeel and Struyf 2002) shows a correlation coefficient of 0.91 between the observed NEA precipitation and that predicted by the physical–statistical model for the period 1994–2012 (Fig. 12a). This high correlation likely comes from a weakening of extratropical variability and a strong connection between EASM and WNP summer monsoon in the recent decades (Lee et al. 2014; Lu et al. 2011; Yim et al. 2008).

As an example, we present the following regression equation for the precipitation anomaly (mm day^{-1}) by using the first 17-yr data as training data:

$$\text{Precipitation} = 0.73A - 0.81B + 0.25C + 0.60D, \quad (1)$$

where A and B use July and June~July averaged data, C is the value determined from July minus June to show the rising tendency, and D is an average of May and June (Fig. 11a). Since all four predictors are normalized, the regression coefficients in this empirical model represent the relative importance of each predictor. From this, the NEA SST is the most important factor, consistent with the highest correlation value in Fig. 6. Cold SST anomalies over NEA ($-B$) are related to an increase in the NEA precipitation. The IO and North Atlantic SST anomalies also play a role, and the CP ENSO–related SST anomaly has the smallest contribution. It should be noted that the relative importance changes slightly according to the training period.

For long-term or seasonal forecasting, only spring data can be used. Since the identified physical predictors evolve with time, the areas for the predictor SST anomalies are slightly modified, as shown in Fig. 11b. The IO SST anomaly uses data for the month of May, and NEA SST uses April~May averaged data; meanwhile, the CP SST anomalies use April-minus-March values in order to utilize the apparent increasing tendency during spring. April data are used for the NAO-related Atlantic SST anomaly. Through a stepwise regression procedure, the following prediction model is established:

$$\text{Precipitation} = 0.82A - 0.72B + 0.50C + 0.68D, \quad (2)$$

where no large differences occur in the coefficients of the predictors, except for the CP SST anomaly and the order-reversed relative importance between A and B. The empirical prediction scheme in Eq. (2) yields a very high correlation score of up to 0.84 (Fig. 12b). As another validation method, a tercile prediction score (i.e., normal, below normal, and above normal) is estimated, based on Gerrity skill score, which allocates greater weight to the correct forecast of nonnormal cases. The Gerrity skill score was 0.65, high enough to utilize in the seasonal forecasting. As previously mentioned, contemporary dynamic forecast models lack prediction skill, so the reliable prediction from the physical–statistical model can be very useful.

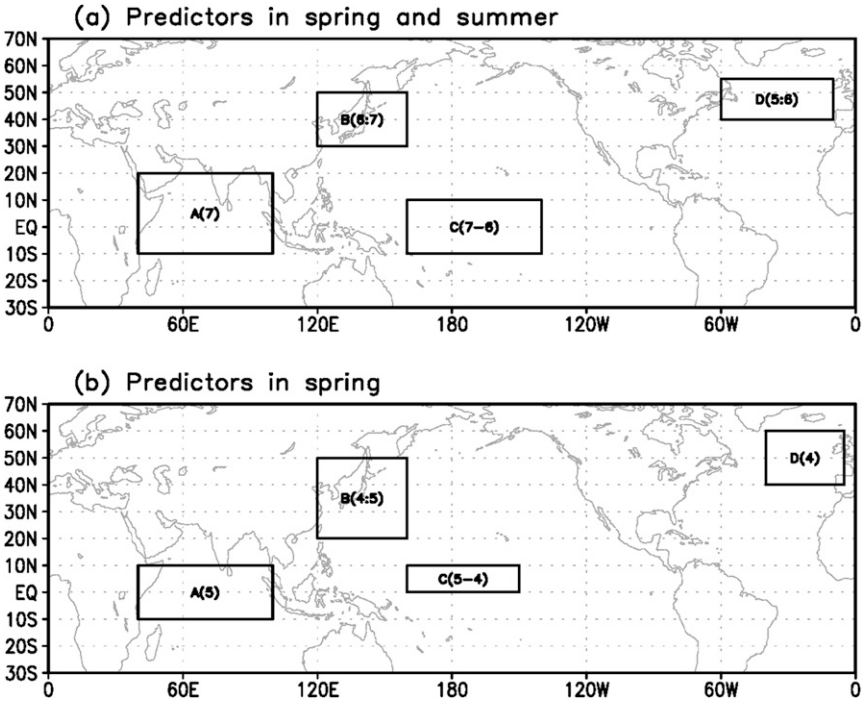

FIG. 11. Domain for the prediction of the July precipitation over NEA using (a) May-to-July predictors and (b) spring predictors. Domain A is the Indian Ocean SST anomaly, B is SST anomaly near NEA, C is CP ENSO–related SST anomaly, and D is the North Atlantic SST anomaly related to NAO. Values in parentheses denote month.

For the sake of stability check, a random 4-yr-out cross-validation method is repeated 10 000 times. The resulting correlations for the prediction from summer and spring are 0.91 and 0.78, respectively. As another test, a random 9-yr-out validation experiment is also performed. The correlations are calculated as 0.90 and 0.74 for summer and spring initial data, respectively, which is considered a reasonable decrease. Therefore, the prediction performance is not highly sensitive to the validation method.

5. Summary and discussion

Prediction of precipitation variation in the NEA region is not easy, partly owing to its distance from rather well-predicted subtropical monsoon systems. This study shows the potential to skillfully predict East Asian July precipitation one season ahead by understanding the physical mechanisms revealed from dominant modes of airmass and monsoonal-front variability near NEA. Use of the large-scale thermodynamic field (i.e., equivalent potential temperature), rather than precipitation or circulation, provides a new perspective on the dominant modes of the EASM. To avoid the general dominance of the tropical variability in meteorological variables, the EOF analysis was performed on a correlation matrix.

The leading three modes show the prominent dynamical linkage to the global sea surface temperature anomalies. The first mode is related to the developing central Pacific El Niño, where diabatic heating over the equatorial central Pacific and cooling over the equatorial western Pacific induce the atmospheric Rossby wave train over the WNP and generate the precipitation over the NEA region. The second mode has a strong interannual relationship with the PDO. In the positive phase of the PDO, atmospheric cold temperature anomaly extends to the eastern Eurasian continent and leads to increases in the meridional gradient of EPT and baroclinicity. The third mode correlates significantly with Indian Ocean warming. The enhanced diabatic heating over the northern Indian Ocean intensifies the mean easterly trade winds over the WNP and strengthens the NPSH via local air–sea interaction. The suppressed convection over the WNP induces the Pacific–Japan teleconnection pattern to increase the precipitation over NEA.

Based on these physical factors, we developed the statistical forecast model for northern East Asian monsoon precipitation in July. The predictors constructed by slowly varying external forcing (like SST anomalies over the central equatorial Pacific, the northwestern Pacific, the Indian Ocean, and the Atlantic) provide a correlation skill of 0.91 for the simultaneous forecast using summer

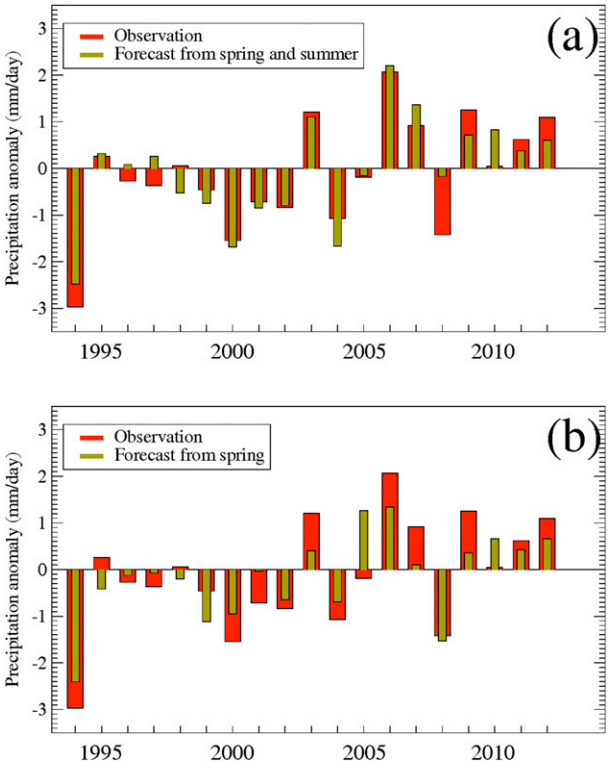

FIG. 12. Observed precipitation anomalies (red bars) over the NEA region and predicted precipitation anomalies (green bars) using predictors from (a) spring and summer and (b) preceding spring.

SST anomalies and 0.84 for the 1-month lead prediction using spring SST anomalies.

The EOF analysis on the correlation and covariance matrix for precipitation or horizontal winds tends to overestimate the impact of tropical and subtropical processes such as the ENSO and WNP subtropical anticyclone, so special caution is required for the study of the EASM (which includes the NEA monsoon). The current analysis using EPT can be applied to other frontal monsoon systems, such as the African, South American, or North American monsoons, and their respective empirical prediction models can be developed.

The approach taken in this study implicitly assumes that the stationary statistics to avoid a climate regime shift (mostly in terms of large-scale circulation fields) occurred in 1993/94. In this regard, the best way to ensure a successful and reliable seasonal forecast is through the use of dynamical models. Recent dynamical models have made much progress in accurately simulating the EASM. For example, compared to the CFSv1 (Yang et al. 2008), the CFSv2 simulated a much more realistic climatological-mean East Asian monsoon rainband (Chen et al. 2013). Thus, dominant physical processes can be revealed with more confidence from sensitivity experiments using dynamical models in the future. However, seasonal prediction skill for monsoon precipitation is still limited in this model, as shown in Chen et al. (2013) and our calculation in Fig. 1. This daunting problem is a subject for future research.

Acknowledgments. This work was funded by the Korea Meteorological Administration Research and Development Program under Grant KMIPA 2015-2113. The authors would like to acknowledge the support from the Korea Institute of Science and Technology Information (KISTI). We thank the three reviewers for their constructive and helpful comments and suggestions.

REFERENCES

Adler, R. F., and Coauthors, 2003: The Version-2 Global Precipitation Climatology Project (GPCP) monthly precipitation analysis (1979–present). *J. Hydrometeor.,* **4,** 1147–1167, doi:10.1175/1525-7541(2003)004<1147:TVGPCP>2.0.CO;2.

Badr, H. S., B. F. Zaitchik, and S. D. Guikema, 2014: Application of statistical models to the prediction of seasonal rainfall anomalies over the Sahel. *J. Appl. Meteor. Climatol.,* **53,** 614–636, doi:10.1175/JAMC-D-13-0181.1.

Blockeel, H., and J. Struyf, 2002: Efficient algorithms for decision tree cross-validation. *J. Mach. Learn. Res.,* **3,** 621–650.

Chang, C.-P., Y. Zhang, and T. Li, 2000: Interannual and interdecadal variations of the East Asian summer monsoon and tropical Pacific SSTs. Part I: Roles of the subtropical ridge. *J. Climate,* **13,** 4310–4325, doi:10.1175/1520-0442(2000)013<4310:IAIVOT>2.0.CO;2.

Chen, J., P. Zhao, S. Yang, G. Liu, and X. Zhou, 2013: Simulation and dynamical prediction of the summer Asian–Pacific Oscillation and associated climate anomalies by the NCEP CFSv2. *J. Climate,* **26,** 3644–3656, doi:10.1175/JCLI-D-12-00368.1.

Czaja, A., and C. Frankignoul, 2002: Observed impact of Atlantic SST anomalies on the North Atlantic Oscillation. *J. Climate,* **15,** 606–623, doi:10.1175/1520-0442(2002)015<0606:OIOASA>2.0.CO;2.

Delworth, T. L., 1996: North Atlantic interannual variability in a coupled ocean–atmosphere model. *J. Climate,* **9,** 2356–2375, doi:10.1175/1520-0442(1996)009<2356:NAIVIA>2.0.CO;2.

Gao, T., and L. Xie, 2014: Multivariate regression analysis and statistical modeling for summer extreme precipitation over the Yangtze River basin, China. *Adv. Meteor.,* **2014,** 269059, doi:10.1155/2014/269059.

Gillies, R. R., S.-Y. Wang, Y. Sun, and O.-Y. Chung, 2013: Supportive empirical modelling for the forecast of monsoon precipitation in Nepal. *Int. J. Climatol.,* **33,** 3047–3054, doi:10.1002/joc.3649.

Jiang, X., S. Yang, J. Li, Y. Li, H. Hu, and Y. Lian, 2013: Variability of the Indian Ocean SST and its possible impact on summer western North Pacific anticyclone in the NCEP Climate Forecast System. *Climate Dyn.,* **41,** 2199–2212, doi:10.1007/s00382-013-1934-2.

Kanamitsu, M., W. Ebisuzaki, J. Woollen, S. K. Yang, J. J. Hnilo, M. Fiorino, and G. L. Potter, 2002: NCEP–DOE AMIP-II Reanalysis (R-2). *Bull. Amer. Meteor. Soc.,* **83,** 1631–1643, doi:10.1175/BAMS-83-11-1631.

Kwon, M., J.-G. Jhun, and K.-J. Ha, 2007: Decadal change in East Asian summer monsoon circulation in the mid-1990s. *Geophys. Res. Lett.,* **34,** L21706, doi:10.1029/2007GL031977.

Latif, M., and T. P. Barnett, 1996: Decadal climate variability over the North Pacific and North America: Dynamics and predictability.

J. Climate, **9,** 2407–2423, doi:10.1175/1520-0442(1996)009<2407:DCVOTN>2.0.CO;2.

Lau, K.-M., K.-M. Kim, and S. Yang, 2000: Dynamical and boundary forcing characteristics of regional components of the Asian summer monsoon. *J. Climate,* **13,** 2461–2482, doi:10.1175/1520-0442(2000)013<2461:DABFCO>2.0.CO;2.

Lee, E.-J., K.-J. Ha, and J.-G. Jhun, 2014: Interdecadal changes in interannual variability of the global monsoon precipitation and interrelationships among its subcomponents. *Climate Dyn.,* **42,** 2585–2601, doi:10.1007/s00382-013-1762-4.

Lee, S.-E., and K.-H. Seo, 2013: The development of a statistical forecast model for changma. *Wea. Forecasting,* **28,** 1304–1321, doi:10.1175/WAF-D-13-00003.1.

Lu, R., H. Ye, and J.-G. Jhun, 2011: Weakening of interannual variability in the summer East Asian upper-tropospheric westerly jet since the mid-1990s. *Adv. Atmos. Sci.,* **28,** 1246–1258, doi:10.1007/s00376-011-0222-5.

Mantua, N. J., S. Hare, Y. Zhang, J. Wallace, and R. Francis, 1997: A Pacific interdecadal climate oscillation with impacts on salmon production. *Bull. Amer. Meteor. Soc.,* **78,** 1069–1079, doi:10.1175/1520-0477(1997)078<1069:APICOW>2.0.CO;2.

Nitta, T., 1987: Convective activities in the tropical western Pacific and their impact on the Northern Hemisphere summer circulation. *J. Meteor. Soc. Japan,* **65,** 373–390.

North, G. R., T. L. Bell, R. F. Cahalan, and F. J. Moeng, 1982: Sampling errors in the estimation of empirical orthogonal functions. *Mon. Wea. Rev.,* **110,** 699–706, doi:10.1175/1520-0493(1982)110<0699:SEITEO>2.0.CO;2.

Overland, J., and R. Preisendorfer, 1982: A significance test for principal components applied to a cyclone climatology. *Mon. Wea. Rev.,* **110,** 1–4, doi:10.1175/1520-0493(1982)110<0001:ASTFPC>2.0.CO;2.

Saha, S., and Coauthors, 2006: The NCEP Climate Forecast System. *J. Climate,* **19,** 3483–3517, doi:10.1175/JCLI3812.1.

Schneider, N., and B. D. Cornuelle, 2005: The forcing of the Pacific decadal oscillation. *J. Climate,* **18,** 4355–4373, doi:10.1175/JCLI3527.1.

Seo, K.-H., and W. Wang, 2010: The Madden–Julian oscillation simulated in the NCEP Climate Forecast System model: The importance of stratiform heating. *J. Climate,* **23,** 4770–4793, doi:10.1175/2010JCLI2983.1.

——, J.-H. Son, S.-E. Lee, T. Tomita, and H.-S. Park, 2012: Mechanisms of an extraordinary East Asian summer monsoon event in July 2011. *Geophys. Res. Lett.,* **39,** L05704, doi:10.1029/2011GL050378.

——, J. Ok, J.-H. Son, and D.-H. Cha, 2013: Assessing future changes in the East Asian summer monsoon using CMIP5 coupled models. *J. Climate,* **26,** 7662–7675, doi:10.1175/JCLI-D-12-00694.1.

Smith, T. M., R. W. Reynolds, T. C. Peterson, and J. Lawrimore, 2008: Improvements to NOAA's historical merged land–ocean surface temperature analysis (1880–2006). *J. Climate,* **21,** 2283–2296, doi:10.1175/2007JCLI2100.1.

Sun, D.-Z., and F. Bryan, 2010: *Climate Dynamics: Why Does Climate Vary? Geophys. Monogr.,* Vol. 189, Amer. Geophys. Union, 216 pp., doi:10.1029/GM189.

Tomita, T., T. Yamaura, and T. Hashimoto, 2011: Interannual variability of the baiu season near Japan evaluated from the equivalent potential temperature. *J. Meteor. Soc. Japan,* **89,** 517–537, doi:10.2151/jmsj.2011-507.

Wang, B., and Z. Fan, 1999: Choice of South Asian summer monsoon indices. *Bull. Amer. Meteor. Soc.,* **80,** 629–638, doi:10.1175/1520-0477(1999)080<0629:COSASM>2.0.CO;2.

——, and LinHo, 2002: Rainy season of the Asian–Pacific summer monsoon. *J. Climate,* **15,** 386–398, doi:10.1175/1520-0442(2002)015<0386:RSOTAP>2.0.CO;2.

——, R. Wu, and X. Fu, 2000: Pacific–East Asian teleconnection: How does ENSO affect East Asian climate? *J. Climate,* **13,** 1517–1536, doi:10.1175/1520-0442(2000)013<1517:PEATHD>2.0.CO;2.

——, Q. Ding, X. Fu, I.-S. Kang, K. Jin, J. Shukla, and F. Doblas-Reyes, 2005: Fundamental challenge in simulation and prediction of summer monsoon rainfall. *Geophys. Res. Lett.,* **32,** L15711, doi:10.1029/2005GL022734.

——, Z. Wu, J. Li, J. Liu, C.-P. Chang, Y. Ding, and G. Wu, 2008: How to measure the strength of the East Asian summer monsoon. *J. Climate,* **21,** 4449–4463, doi:10.1175/2008JCLI2183.1.

——, B. Xiang, and J.-Y. Lee, 2013: Subtropical high predictability establishes a promising way for monsoon and tropical storm predictions. *Proc. Natl. Acad. Sci. USA,* **110,** 2718–2722, doi:10.1073/pnas.1214626110.

Watanabe, M., and M. Kimoto, 2000: Atmosphere-ocean thermal coupling in the North Atlantic: A positive feedback. *Quart. J. Roy. Meteor. Soc.,* **126,** 3343–3369, doi:10.1002/qj.49712657017.

Webster, P. J., V. O. Magaña, T. N. Palmer, J. Shukla, R. A. Tomas, M. Yanai, and T. Yasunari, 1998: Monsoons: Processes, predictability, and the prospects for prediction. *J. Geophys. Res.,* **103,** 14 451–14 510, doi:10.1029/97JC02719.

Wu, Z., B. Wang, J. Li, and F.-F. Jin, 2009: An empirical seasonal prediction model of the East Asian summer monsoon using ENSO and NAO. *J. Geophys. Res.,* **114,** D18120, doi:10.1029/2009JD011733.

Xie, S.-P., K. Hu, J. Hafner, H. Tokinaga, Y. Du, G. Huang, and T. Sampe, 2009: Indian Ocean capacitor effect on Indo–western Pacific climate during the summer following El Niño. *J. Climate,* **22,** 730–747, doi:10.1175/2008JCLI2544.1.

Yang, J., Q. Liu, S.-P. Xie, Z. Liu, and L. Wu, 2007: Impact of the Indian Ocean SST basin mode on the Asian summer monsoon. *Geophys. Res. Lett.,* **34,** L02708, doi:10.1029/2007GL030526.

Yang, S., Z. Zhang, V. E. Kousky, R. W. Higgins, S.-H. Yoo, J. Liang, and Y. Fan, 2008: Simulations and seasonal prediction of the Asian summer monsoon in the NCEP Climate Forecast System. *J. Climate,* **21,** 3755–3775, doi:10.1175/2008JCLI1961.1.

Yeh, S.-Y., J.-S. Kug, B. Dewitte, M.-H. Kwon, B. P. Kirtman, and F.-F. Jin, 2009: El Niño in a changing climate. *Nature,* **461,** 511–514, doi:10.1038/nature08316.

Yim, S.-Y., S.-W. Yeh, R. Wu, and J.-G. Jhun, 2008: The influence of ENSO on decadal variations in the relationship between the East Asian and western North Pacific summer monsoons. *J. Climate,* **21,** 3165–3179, doi:10.1175/2007JCLI1948.1.

Zhao, P., X. Zhang, X. Zhou, M. Ikeda, and Y. Yin, 2004: The sea ice extent anomaly in the North Pacific and its impact on the East Asian summer monsoon rainfall. *J. Climate,* **17,** 3434–3447, doi:10.1175/1520-0442(2004)017<3434:TSIEAI>2.0.CO;2.

——, Y.-N. Zhu, and R.-H. Zhang, 2007: An Asian–Pacific teleconnection in summer tropospheric temperature and associated Asian climate variability. *Climate Dyn.,* **29,** 293–303, doi:10.1007/s00382-007-0236-y.

——, S. Yang, and R. Yu, 2010: Long-term changes in rainfall over eastern China and large-scale atmospheric circulation associated with recent global warming. *J. Climate,* **23,** 1544–1562, doi:10.1175/2009JCLI2660.1.